Int. J. Nonlinear Anal. Appl. In Press, 1–20
ISSN: 2008-6822 (electronic)
http://dx.doi.org/10.22075/ijnaa.2026.40857.5669

Stochastic approach for optimal multi-objective energy management of multi-energy Microgrids incorporating a time-of-use-based demand response program

Golamreza Salehi*, Mir-Mohammad Mir-Mousavi, Afshin Mohseni Arasyeh, Hassan Feshki Farahani, Kamran Lari

Department of Mechanical Engineering, CT.C., Islamic Azad University, Tehran, Iran

(Communicated by Saman Babaie-Kafaki)

Abstract

The growing adoption of distributed and renewable energies has significantly improved the sustainability of multi-energy microgrids (MEMGs). This research presents a novel stochastic model for optimal energy management of MEMGs featuring different energy sources, including electricity, heat and storage systems, by addressing uncertainties related to renewables and load in grid-connected and islanded modes while decreasing emissions and operational costs. The proposed optimal energy management system (EMS) incorporates a demand response program (DRP) along with a time-of-use (TOU) pricing model to enhance efficiency and reduce costs and emissions. Given the conflicting nature of the cost and emission minimization objectives, a multi-objective particle swarm optimization (MOPSO) algorithm is formulated to generate the Pareto optimal front. Furthermore, a fuzzy decision-making mechanism is applied to determine the best compromise solution. To achieve this goal, various scenarios are analyzed based on stochastic scheduling of thermal and power resources. However, due to the volume of simulation outputs, results are demonstrated for the most probable case. The total daily cost and emissions are presented for three case studies: (i) grid-connected case, (ii) islanded case, and (iii) time of use (TOU)–based DRP in the grid-connected case. The obtained results revealed that the minimization of operational cost and emission cost in Case B is improved by 9.7% and 15.3% compared to Case A. However, integrating TOU-DRP into EMS (i.e., Case C) has led to 3.25% and 1.37% improvements in operational costs and emissions, respectively, compared to Case B without the inclusion of DRP.

Keywords: Multi-energy microgrid, CHP, emission reduction, operational cost reduction, renewable energy sources, uncertainties, MOPSO, TOU-DRP
2020 MSC: Primary 90C29; Secondary 90C15, 90B35

Highlights

- Proposing a stochastic model for optimum energy management of multi-energy microgrids featuring various components, including WT, PV, CHP, PO, HO, FC, ESS, and HS.
- Considering uncertainties related to the predicted values of load variations and output power of renewables (i.e., WTs and PV units).

*Corresponding author
Email addresses: gh.salehi@iauctb.ac.ir (Golamreza Salehi), mirmohammad12@yahoo.com (Mir-Mohammad Mir-Mousavi), mohseniarasyeh135@yahoo.com (Afshin Mohseni Arasyeh), hassanfeshkifarahani@gmail.com (Hassan Feshki Farahani), larikamran@yahoo.com (Kamran Lari)

Received: April 2026 *Accepted:* June 2026

- Incorporating time-of-use (TOU)-based demand response program (TOU-DPR).
- Presenting multi-objective optimization framework regarding contrasting objectives.

1 Introduction

1.1 Background and Motivation

Amidst the escalating global energy demand and the push toward sustainability, multi-energy microgrids (MEMGs) featuring renewable resources such as wind and solar have emerged as a promising and sustainable paradigm for advance energy management and play a crucial role in reducing carbon emissions and enhancing energy security [7]. However, inherent uncertainties related to renewables present considerable challenges for grid stability and efficiency. Thus, the implementation of an optimum energy management system (EMS) for MEMGs powered by renewable energy sources (RESs) is a key strategy in modern power systems [6, 16, 25, 29]. Thus, by integrating heterogeneous energy carriers including diverse RES units, energy storage systems (ESSs) and combined heat and power (CHP) units, MEMGs not only enhance overall energy efficiency but also play a critical role in mitigating carbon emissions and fostering environmental sustainability. Nevertheless, the optimum operation of MEMGs is inherently complex, primarily due to stochastic nature of renewable generation. To address these multifaceted challenges, advanced optimization techniques have gained prominence as powerful tools for efficient energy coordination. In addition, the widespread use of solar and wind energy is constrained by the high cost and limited capacity of ESSs [36]. As a result, the demand response program (DRP) on the customer side is primarily aimed by different users with substantial electricity needs. Thus, individual customers are expected to take part in DRP to support the growth of RESs. The incorporation of DRP strategies within these frameworks enables load flexibility and cost minimization and improved energy utilization, thereby ensuring efficient allocation of distributed resources under uncertain operating conditions [2, 15]. Moreover, state-of-the-art optimization algorithms facilitate real-time decision-making by considering intermittency, storage availability, and DRP strategy [22, 5]. It should be noted that an efficient EMS not only manage its own assets but also coordinate with neighboring MGs to align generation and consumption, while accounting for the inherent variability of renewable energies. MGs may often be disconnected from the main grid due to factors such as outages, reduced power quality, or planned maintenance. In such cases, the integration of ESSs and RES-based distributed generations (DGs), alongside demand-responsive (DR) loads, provides a practical solution to enhance reliability, reduce emissions, and lower operating costs. Recent studies have been reviewed to highlight existing advancements, research gaps and unresolved challenges.

Therefore, a comprehensive stochastic optimization framework for integrated energy management of MEMGs incorporating DRP is essential [35]. This framework must be equipped to address inherent intermittencies and uncertainties while employing advanced decision-making strategies to ensure the optimum coordination of heterogeneous energy resources under complex operating environments. Within this scope and given the inherent uncertainties associated with RESs and a critical need for models that can reliably coordinate the operation of CHP units, ESSs, and DRP strategies, the present study is dedicated to developing and analyzing optimization model for EM in MEMGs with particular emphasis on cost assessments. To address these challenges, this research work introduces a novel stochastic approach based on multi-objective particle swarm optimization (MOPSO) which is specifically designed to handle the complexity of multi-objective optimization problems.

1.2 Literature Survey

In recent years, considerable progress has been achieved in the field of MG energy management. Several modeling and optimization approaches have been proposed to address the integration of diverse energy resources. Conventionally, optimization techniques including linear programing (LP), non-linear programming (NLP), mixed-integer programming (MILP), and dynamic programing (DP) have been applied to optimize key operational aspects of MGs, including economic dispatch and energy source allocation [33, 30, 12, 20, 19, 34, 13]. In [19], a stochastic scheduling framework is introduced for hybrid multi-area MGs working in islanded mode. The model aimed to reduce operational costs and minimize supply interruptions through coordinated management of resources such as RES, battery ESS (BESS), and electric vehicles (EVs). Collectively, these traditional methodologies have made valuable contributions to the development of comprehensive EM frameworks for MGs, each offering distinct strength and analytical insights. Nevertheless, the principal limitation of these classical approaches lies in their restricted capability to effectively model and solve highly non-linear, non-convex, and dynamic optimization problems inherent in modern MGs. Consequently, recent trends have increasingly focused on application of metaheuristic optimization algorithms to overcome these challenges [9]. These algorithms provide robust and flexible search capabilities, making them well-suited for addressing the

multi-objective and highly complex nature of MG energy management problems. Ref. [18] presented an advanced EMS that integrates model predictive control and fuzzy logic for multi-energy MGs disconnected from the main grid. The system comprised PV units, fuel cells (FCs), batteries, electrolysers, boilers or heat-only (HO) units, hydrogen storage, and thermal loads. Although the hybrid MPC–fuzzy design successfully minimized energy use, its robustness is questionable under highly dynamic and large-scale operational conditions. Authors in [16] worked on a demand-side management (DSM) framework intended to enhance consumer satisfaction while reducing electricity prices in MGs with various tariffs. While it achieved improved economic outcomes, the approach paid less attention to grid reliability and system scalability. Ref. [25] reported a two-layer energy management model for clusters of MGs. The strategy guaranteed spinning reserves to prevent load shedding and relied on demand-side flexibility and shared battery storage to minimize both emissions and operational expenses. More recent literature reported the importance of addressing inherent uncertainties and integrating DRPs into the optimization framework [3, 8, 32, 36]. In [36], authors investigated optimal scheduling in MGs with a focus on DR detection at the customer side. They proposed a master–slave management architecture to balance the economic objectives of MGs with upper-level system constraints. To overcome problems of missing or mislabeled demand data, they adopted machine learning classifiers. Although effective, this solution requires extensive labeled datasets and may suffer from overfitting and weak generalization. Authors in [32] proposed an optimum framework for MG planning incorporating renewable RESs, ESSs, and DRPs. They used the probability density functions (PDFs) as one of the simplest tools to deal with the stochasticity in order to model uncertain parameters. It should be mentioned that the adoption of dynamic pricing mechanisms and incentive-based schemes within MGs has proven effective in promoting more responsible and flexible energy consumption behaviors among end-users. Nevertheless, despite their clear benefits for both MG operators and consumers, DRPs introduce additional layers of complexity into MG EMS [21].

1.3 Research Gap, Contributions, and Organization

A comprehensive survey of the literature on energy planning and management within MEMGs reveals that substantial progress has been achieved in optimizing ESSs and managing RESs. Although numerous studies have addressed energy management in MGs, most existing models lack integration of key aspects such as uncertainty modeling of renewables and load, simultaneous optimization of multiple energy resources of MGs and comprehensive TOU-based DRP under grid-connected conditions. To overcome these limitations, this research work makes the following contributions:

- **Integrated Energy Management Framework for multi-energy microgrid (MEMGs):** unlike conventional approaches that treat electrical and thermal systems in MEMGs separately, the proposed model not only optimizes the operation of CHP units simultaneously, but also considers ESSs, heat storage (HS), wind turbine (WT) and photovoltaic (PV) units.
- **Price-based demand response program:** time-of-use (TOU)-based DRP is incorporated as an effective mechanism for enhancing economic efficiency and operational flexibility. Its joint implementation with optimization strategies remains largely unexplored in the literature,
- **Stochastic Model:** unlike previous studies that rely on deterministic or linear models, the framework accounts for uncertainties in renewable energy generation by incorporating scenario-based stochastic programming, thereby improving system robustness and reliability,
- **Multi-objective Formulation for minimization of two contrasting objectives:** the model minimizes two objectives that are contrasting by nature: (i) operational costs and (ii) emissions, achieving a balanced trade-off between different objectives,

Finally, while several research works reported in the literature have assessed the economic and environmental implications of MEMGs, few have undertaken truly multidimensional evaluations that simultaneously encompass economic and environmental dimensions. Such comprehensive analyses are essential to support strategic decision-making regarding investment and policy formulation for the sustainable development of MG infrastructures.

The remainder of this paper is structured as follows: **Section 2** provides a MEMG components modeling along with the formulation of objective functions and related constraints. **Section 3** focuses on the proposed solution for the optimization problem using MOPSO. **Section 4** presents the case studies and simulations followed by numerical results and discussions. Finally, **Section 5** concludes the paper with key remarks and suggestions for future research.

2 Problem Formulation

Microgrids offer a promising solution for improving energy efficiency, reducing operational costs and enhancing system flexibility. By integrating CHP systems, MGs can simultaneously generate electricity and thermal energy, increasing overall system utilization. Moreover, by recovering waste heat from electricity generation processes, CHP-based systems can significantly lower fuel consumption and emissions. Due to environmental impact of fossil fuel-based generation, it is essential to minimize emissions even though this objective often conflicts with cost reduction. Therefore, the operation of MGs in this research work is formulated as a multi-objective optimization problem, aiming to simultaneously minimize operational cost and pollutant emissions. Multiple power and heat generation units and storage systems such as CHP, FC, ESS, HS units, power-only (PO) and heat-only (HO) units in the MGs are considered. The structure of two types of CHP-based MG system is shown in Figure 1 [17]. In this way, a multi-objective optimization problem is achieved when connected to the network and islanded from the network.

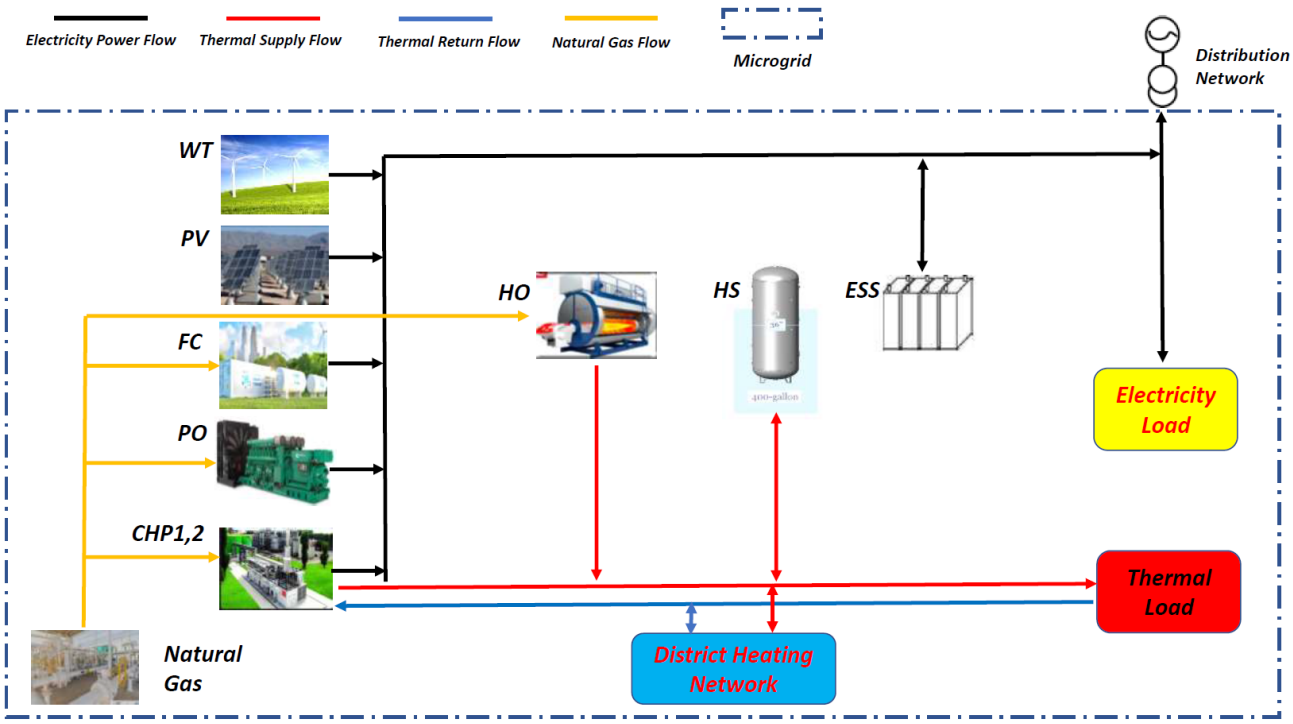


Figure 1: Structure of the CHP-based microgrid system.

2.1 Multi-Energy Microgrid Components Modeling

2.1.1 Uncertainty Modeling by a Scenario-Based Approach

In this study, the inherent uncertainties in the MEMG are addressed through solving an optimum power planning framework. The proposed stochastic model incorporates three main uncertain parameters: (i) wind speed for WT power, (ii) solar irradiance for PV power, and (iii) load demand. The uncertainties associated with these parameters are represented using their continuous PDFs [11, 10]. To capture the variability of these factors, a scenario-based approach is employed, generating a diverse set of scenarios derived from the combinations of these parameters. The overall structure of the proposed stochastic framework is illustrated in following sub-sections.

2.1.2 Scenario Generation and Reduction

Uncertainties are modeled based on their associated prediction errors, which follow PDFs. Figure 2 illustrates a typical continuous PDF for load prediction error, along with its discretized form [27]. In scenario-based stochastic programming, a continuous random variable is represented by a finite number of discrete scenarios, each with an associated probability. In this research, three uncertain variables are modeled using a three-level discretization of the respective PDFs: (i) WT output power, (ii) PV output power, and (iii) load demand. Each level represents a distinct scenario with an associated probability, resulting in a simplified yet statistically representative model of the underlying

randomness. The continuous PDFs of these variables are used to generate the uncertainties of these parameters; then, the scenario-based method is utilized for generating a set of scenarios from combinations of these parameters.

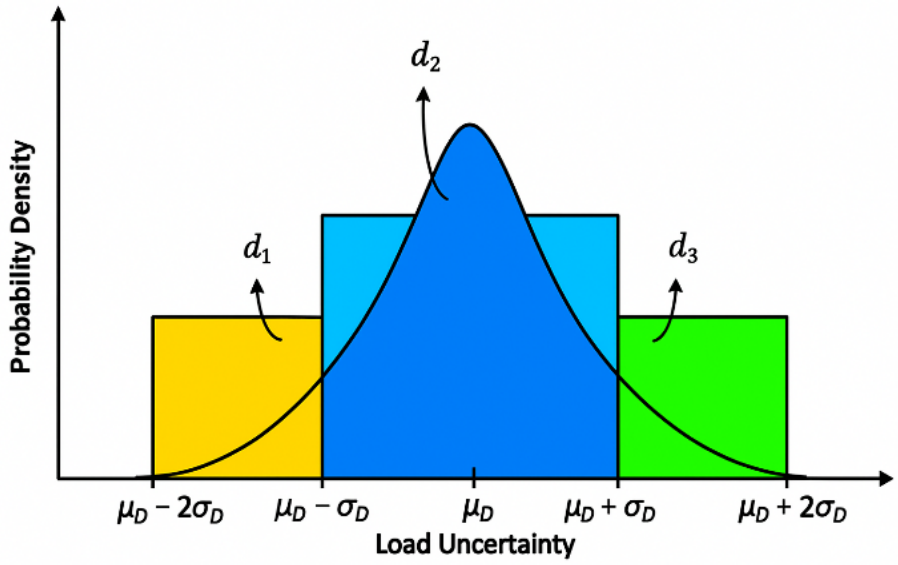


Figure 2: Typical discretization of a probability density function for load prediction error.

To reduce computational complexity and the execution time of the proposed algorithm, a backward scenario reduction technique is employed [27]. This technique preserves the required accuracy of the stochastic model while significantly decreases the number of scenarios to be processed, thus accelerating the optimization process. Scenario reduction involves selecting a representative subset of the full scenario set, such that the statistical characteristics of the original uncertainty distributions are retained. The simultaneous backward reduction method follows five steps.

Step 1	**Initialization**	**Define:** S as the initial set of scenarios and DS as the initially empty discarded-scenario set. **Compute:** $DT_{s,s'} = DT(\xi_s, \xi_{s'})$, $s, s' = 1, 2, \ldots, N_s$, where $DT_{s,s'} = \sqrt{\sum_{i=1}^{d} (v_i^s - v_i^{s'})^2}$.
Step 2	**Evaluation**	For each scenario k, compute $DT_{k,r} = \min(DT_{k,s'})$, $s', k \in S$, $s' \neq k$; r is the scenario index having minimum distance from scenario k.
Step 3	**Elimination**	Calculate $PD_{k,r} = \pi_k DT_{k,r}$, $k \in S$. Select d such that $PD_d = \min(PD_k)$, $k \in S$.
Step 4	**Update**	Set $S = S - \{d\}$, $DS = DS \cup \{d\}$, and $\pi_r = \pi_r + \pi_d$.
Step 5	**Iteration**	Repeat Steps 2–4 until the desired number of scenarios remains.

Let $\xi_s (s = 1, 2, \ldots, N_s)$ be the initial set containing N_s scenarios, each with an associated probability π_s and $DT_{s,s'}$ be the distance between a pair of scenarios (s, s').

2.1.3 Wind Turbine (WT) Power Modeling

The wind speed variability is modeled using Weibull distribution ($f_v(v)$) widely used for wind energy potential. The Weibull function is characterized by two main parameters: (i) parameter k that is associated to the shape of Weibull distribution, (ii) parameter c that is related to the dispersion of Weibull distribution [4]. These parameters are generally estimated through a variety of techniques, including maximum likelihood estimation (MLE), the method of moments, the least squares approach, etc. Once these parameters are obtained, the fitted Weibull distribution serves as a statistical model for wind speed behavior and is used to estimate potential energy output. The core mathematical representations of the Weibull distribution are given as PDF by Eq. (1) and the output power of WT is characterized by Eq. (2), the generated wind speeds and their probabilities can be presented by Eqs. (3) and (4) [28, 15].

$$f_v(v) = \left(\frac{k}{c}\right)\left(\frac{v}{c}\right)^{k-1} \exp\left[-\left(\frac{v}{c}\right)^{k}\right], \qquad 0 \leq v < \infty \tag{2.1}$$

$$P_{WT}(v) = \begin{cases} 0, & v < v_{ci} \text{ or } v > v_{co}, \\ P_{WT}^{\text{Rated}} \left(\dfrac{v_{co} - v_{ci}}{v_R - v_{ci}} \right), & v_{ci} \le v \le v_R, \\ P_{WT}^{\text{Rated}}, & v_R \le v \le v_{co}, \end{cases} \tag{2.2}$$

$$\pi_{\text{wind},z} = \int_{v_z^{\min}}^{v_z^{\max}} \left(\frac{k}{c} \right) \left(\frac{v}{c} \right)^{k-1} e^{-(v/c)^z} \, dv \tag{2.3}$$

$$v_z = \frac{1}{\pi_{\text{wind},z}} \int_{v_z^{\min}}^{v_z^{\max}} \left(\frac{k}{c} \right) \left(\frac{v}{c} \right)^{z-1} e^{-(v/c)^z} \, dv \tag{2.4}$$

where f_v is the Weibull PDF of wind speed, k and c are shape and scale parameters of Weibull function, v_{ci}, v_{co} and v_{R} are the cut-in, cut-out and rated wind speed of WT, respectively, P_{WT} and P_{WT}^{Rated} are the output power and the rated power of WT, respectively, $\pi_{wind,z}$ is the probability of the wind speed in z-th interval, $v_z^{\min}$ and $v_z^{\max}$ denote the starting and ending points of wind speed's interval in z-th scenario, respectively.

Overall, three scenarios of wind speed are generated from previous equations in this research work. The wind speed scenarios and their probabilities are listed in Table 1 for $k = 2.5034$ and $c = 10.0434$ [28].

2.1.4 Photovoltaic (PV) Unit Power Modeling

Solar irradiance uncertainty is modeled using Beta distribution ($f_G(G)$), that is particularly suitable for bounded variables like irradiance. The related PDF is defined by Eqs. (5), (6) and (7), and the PV unit output power can be described by Eq. (8). Three scenarios are obtained from above formulations by dividing the PDF into three intervals. The solar irradiance probability is expressed by Eq. (9) while its corresponding solar irradiance for each scenario is represented by Eq. (10) [28].

$$f_G(G) = \begin{cases} \dfrac{\Gamma(\alpha + \beta)}{\Gamma(\alpha) + \Gamma(\beta)} G^{\alpha-1} (1 - G)^{\beta-1}, & 0 \le G \le 1, \ 0 \le \alpha, \beta, \\ 0, & \text{otherwise}, \end{cases} \tag{2.5}$$

$$\beta = (1 - \mu_s) \left(\frac{\mu_s (1 + \mu_s)}{\sigma_s^2} \right) - 1 \tag{2.6}$$

$$\alpha = (1 - \mu_s) \left(\frac{\mu_s \beta}{1 - \mu_s} \right) - 1 \tag{2.7}$$

$$P_s(G) = \begin{cases} P_{sr} \left(\dfrac{G^2}{G_{\text{std}} X_c} \right), & 0 < G \le X_c, \\ P_{sr} \left(\dfrac{G}{G_{\text{std}}} \right), & G \ge X_c, \end{cases} \tag{2.8}$$

$$\pi_{\text{solar},m} = \int_{G_m^{\min}}^{G_m^{\max}} f_G(G) \, dG \tag{2.9}$$

$$G_m = \frac{1}{\pi_{\text{solar},m}} \int_{G_m^{\min}}^{G_m^{\max}} \frac{\Gamma(\alpha + \beta)}{\Gamma(\alpha) + \Gamma(\beta)} G^{\alpha-1} (1 - G)^{\beta-1} \, dG \tag{2.10}$$

where f_{G} is the Beta PDF of solar irradiance, α and β are parameters of Beta function, G is solar irradiance, μ_{s} is mean of the solar irradiation for each time interval, P_{s} and P_{sr} are the output and rated power of PV unit, respectively, X_c is a certain irradiance point, G_{std} is a standard environment solar irradiance, $\pi_{solar,m}$ is the probability of the solar irradiance in m-th interval, $G_m^{\min}$ and $G_m^{\max}$ denote the starting and ending point of solar irradiance's interval in m-th scenario, respectively.

G_{std} is set to be 1000W/m^2, and X_c is set to be 120 W/m^2. The probabilities and generated scenarios of the solar irradiance are provided in Table 1 for $\alpha = 6.38$ and $\beta = 3.43$.

2.1.5 Load-Demand Modeling

The uncertainty in load demand is modeled using Normal (Gaussian) distribution ($f_{\mathrm{d}}(P_{\mathrm{d}})$). The load variations are assumed to follow a Normal distribution comprising of two main parameters of mean (μ) and standard deviation (σ). The PDF of the load demand is expressed by Eq. (11), the probabilities and generated load scenarios obtained from Eq. (11) can be described by Eqs. (12) and (13) [28].

$$f_d(P_d) = \frac{1}{\sigma_d\sqrt{2\pi}} \exp\left[-\frac{(P_d-\mu_d)^2}{2\sigma_d^2}\right] \tag{2.11}$$

$$\pi_{d,i} = \int_{P_{d,i}^{\min}}^{P_{d,i}^{\max}} \frac{1}{\sigma_d\sqrt{2\pi}} \exp\left[-\frac{(P_d-\mu_d)^2}{2\sigma_d^2}\right] dP_d \tag{2.12}$$

$$P_{d,i} = \frac{1}{\tau_{d,i}} \int_{P_{d,i}^{\min}}^{P_{d,i}^{\max}} \frac{P_d}{\sigma_d\sqrt{2\pi}} \exp\left[-\frac{(P_d-\mu_d)^2}{2\sigma_d^2}\right] dP_d \tag{2.13}$$

where f_{d} is the Normal PDF of load demand, μ_d and σ_d are parameters of Normal function of load demand, $\pi_{d,i}$ is the probability of the load demand in i-th interval, $P_{d,i}^{\min}$ and $P_{d,i}^{\max}$ denote the maximum and minimum limit of the selected interval i, respectively.

In this study, three load scenarios obtained by dividing the Normal PDF into three intervals. The probabilities and load scenarios when $\mu_{\mathrm{d}} = 70$ and $\sigma_{\mathrm{d}} = 10$, are provided in Table 1.

Table 1: Generated scenarios for uncertain WT, PV, and load-demand parameters.

Scenario / category	Probability	Value
1	0.1587	54.7486
2	0.6827	70.0000
3	0.1587	85.2514
Wind Scenario		Wind Speed (m/s)
1	0.7902	7.4518
2	0.1694	13.6153
3	0.0404	17.7289
Irradiance Scenario		Solar Irradiance (w/m2)
1	0.1605	416.0627
2	0.4412	609.1166
3	0.3983	790.4621

2.1.6 Combined Scenario Modeling for WT, PV, and Load Demand

To simultaneously capture the impact of uncertainties in WT, PV, and load demand, the probabilities of the related parameters are multiplied by Eq. (14). As a result, a total of 27 combined scenarios are generated from Eq. (14). Table 2 presents the obtained scenarios and the associated values of the uncertain parameters and their joint probabilities.

$$\pi_S = \pi_{d,i}\,\pi_{\mathrm{wind},k}\,\pi_{\mathrm{solar},m} \tag{2.14}$$

where π_{s} is the combined probabilities of scenarios.

2.1.7 Combined Heat and Power (CHP) Unit Modeling

Two types of CHP units in MEMG have been included in this paper and the feasible operating regions (FOR) for each type are shown in Figure 3. CHP's electrical and thermal production outputs must be located in the enclosed area, formed by points A, B, C, D, E and F. More details in this regard are available in [26]. Total operation cost of a CHP related to both heat and electricity is modeled by Eq. (15).

$$C(P_h^{CHP}, H_h^{CHP}) = a(P_h^{CHP})^2 + bP_h^{CHP} + c + d(H_h^{CHP})^2 + eH_h^{CHP} + fH_h^{CHP}P_h^{CHP} \tag{2.15}$$

where C denotes cost, P_h^{CHP} and H_h^{CHP} denote the generated power and heat the CHP, respectively, a, b, c, d, e, and f are cost function coefficients of CHP units.

Table 2: Combined scenarios and probabilities for WT, PV, and load demand.

Scenario	Loading (%)	Wind speed (m/s)	Solar irradiance (W/m^2)	$\pi_{d,i}$	$\pi_{\text{wind},z}$	$\pi_{\text{solar},m}$	π_S
S1	54.7486	7.4518	416.0627	0.1587	0.7902	0.1605	0.0201
S2	54.7486	13.6153	416.0627	0.1587	0.1694	0.1605	0.0043
S3	54.7486	17.7289	416.0627	0.1587	0.0404	0.1605	0.0010
S4	54.7486	7.4518	609.1166	0.1587	0.7902	0.4412	0.0553
S5	54.7486	13.6153	609.1166	0.1587	0.1694	0.4412	0.0119
S6	54.7486	17.7289	609.1166	0.1587	0.0404	0.4412	0.0028
S7	54.7486	7.4518	790.4621	0.1587	0.7902	0.3983	0.0499
S8	54.7486	13.6153	790.4621	0.1587	0.1694	0.3983	0.0107
S9	54.7486	17.7289	790.4621	0.1587	0.0404	0.3983	0.0026
S10	70.0000	7.4518	416.0627	0.6827	0.7902	0.1605	0.0866
S11	70.0000	13.6153	416.0627	0.6827	0.1694	0.1605	0.0186
S12	70.0000	17.7289	416.0627	0.6827	0.0404	0.1605	0.0044
S13	70.0000	7.4518	609.1166	0.6827	0.7902	0.4412	0.2380
S14	70.0000	13.6153	609.1166	0.6827	0.1694	0.4412	0.0510
S15	70.0000	17.7289	609.1166	0.6827	0.0404	0.4412	0.0122
S16	70.0000	7.4518	790.4621	0.6827	0.7902	0.3983	0.2149

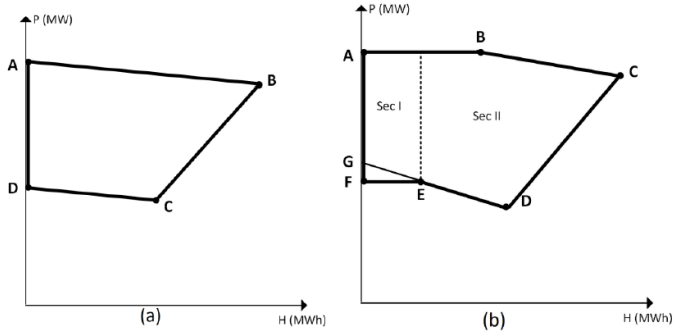


Figure 3: Feasible operating regions for CHP units: (a) Type 1 and (b) Type 2.

2.1.8 Power-Only (PO) and Heat-Only (HO) Unit Modeling

Power-only and heat-only (HO) units are considered in MEMG to produce only electricity and heat when required, respectively. Operation constraints of PO and HO units are expressed by (16) and (17), respectively. And, cost functions of PO and HO units are represented by (18) and (19), respectively.

$$P_h^{PO-\min} V_h^{PO} \leq P_h^{PO} \leq P_h^{PO-\max} V_h^{PO} \tag{2.16}$$

$$H_h^{HO-\min} V_h^{HO} \leq H_h^{HO} \leq H_h^{HO-\max} V_h^{HO} \tag{2.17}$$

$$C(P_h^{PO}) = \lambda_{PO} P_h^{PO} \tag{2.18}$$

$$C(H_h^{HO}) = \lambda_{HO} H_h^{HO} \tag{2.19}$$

where P_h^{PO} is generated power of PO in h-th hour (MW), $P_h^{P0-min}$and P_h^{PO-max} are minimum and maximum power limit of PO unit, respectively, H_h^{HO} is generated heat of HO unit in h-th hour (MWth), $H_h^{HO-min}$and H_h^{HO-max} are minimum and maximum heat limit of HO unit, respectively, $C\left(P_h^{PO}\right)$ is cost function of PO unit, λ_{PO} denotes the power price of PO unit in h-th hour (\$/MWh), $C\left(H_h^{HO}\right)$ is cost function of HO unit, and λ_{HO} is the heat price of HO unit in h-th hour (\$/MWh).

2.1.9 Fuel Cell (FC) Unit Modeling

Fuel cell (FC) is considered as a power production unit, which can generate electricity from natural gas and methanol hydrogen-containing fuel. The cost of an FC unit is expressed by Eq. (20) [31].

$$C_{FC} = \sum_{t=1}^{T} \left(\beta_{\text{natural}} \sum_{i=1}^{N_{FC}} \frac{P_{FC,it}}{\eta_{FC,ei}} + \frac{H_{FC,it}}{\eta_{FC,hi}} \right) \tag{2.20}$$

where C_{FC} is the FC generation cost, $\beta_{natural}$ is the natural gas cost in \$/Kg, $P_{FC,it}$ and $H_{FC,it}$ are the FC electricity and heat generation of the i-th unit in time-t, respectively, $\eta_{FC,ei}$ and $\eta_{FC,hi}$ are the FC electricity and heat efficiency of i-th unit, respectively, N_{FC} is the number of FC plants.

2.1.10 Electrical Energy Storage (ESS) Modeling

The charge and discharge modes of electrical energy storage (ESS) are modeled by Eqs. (21-26). It can be seen in Eq. (21) that the state of charge (SOC) in each hour is obtained by considering the charging and discharging amounts of the ESS in that hour. Based on Eq. (22), the SOC at the beginning and the end times must be equal. The SOC is limited by its bound in (23). The amount of charging/discharging is limited to the maximum capacity of the ESS by (24) and (25). According to (26), the charging and discharging modes cannot occur simultaneously.

$$SOC(t) = SOC(t-1) + P^{ch}(t)\eta_{ch}^{ST} - \frac{P^{dch}(t)}{\eta_{Dch}^{ST}} \tag{2.21}$$

$$SOC(t_0) = SOC(t_T) \tag{2.22}$$

$$E_{\min}^{st} \le SOC(t) \le E_{\max}^{st} \tag{2.23}$$

$$P^{dch}(t) \le E_{\max}^{Dch}\,\zeta_{dch} \tag{2.24}$$

$$P^{ch}(t) \le E_{\max}^{st}\,\zeta_{ch} \tag{2.25}$$

$$\zeta_{ch} + \zeta_{dch} \le 1 \tag{2.26}$$

where $SOC(t)$ is the state-of-charge of ESS in time-t, η_{ch}^{ST} and η_{Dch}^{ST} are the ESS charging and discharging efficiencies, respectively; P^{ch} and P^{dch} are the charged and discharged power of ESS, respectively; $E_{\min}^{st}$ and $E_{\max}^{st}$ are the minimum and maximum capacity of the ESS, respectively; ζ_{ch} and ζ_{dch} are binary variables representing the charge/discharge state of ESS, respectively.

2.1.11 Heat Storage (HS) Modeling

The total generated heat is calculated by Eq. (27). heat losses during start-up and shut-down periods can be modeled by (28). The available heat capacity at each time interval in the heat storage (HS) is expressed by Eq. (29). By (30), the maximum available capacity of HS can be limited. The ramping up/down rates for the HS system are modeled by (31) and (32).

$$H_h = \sum_{i=1}^{N_{CHP}} H_{i,h}^{CHP} + H_h^{HO} + H_h^{FC} \tag{2.27}$$

$$H_h = \overline{H_h} - \beta_{\text{loss}} SU_h^i + \beta_{\text{gain}} SD_h^i, \qquad i \in \{FC, CHP, HO\} \tag{2.28}$$

$$B_h = (1-\eta)B_{h-1} + H_h - H_h^{\text{load}} \tag{2.29}$$

$$B_{\min} \le B_h \le B_{\max} \tag{2.30}$$

$$B_{h-1} - B_h \le B_{\max}^{\text{charge}} \tag{2.31}$$

$$B_{h-1} - B_h \le B_{\max}^{\text{discharge}} \tag{2.32}$$

where, H_{h} denotes total generated heat, $H_{i,h}^{CHP}$, H_h^{HO}, and H_h^{FC} are heat generated by CHP, HO and FC, respectively, β_{loss} and β_{gain} denote heat generation loss/gain of the CHP unit during startup/shutdown period, η is heat loss rate of the HS, $B_{\min}$ and $B_{\max}$ are minimum and maximum HS capacity in MW, respectively, $B_{\max}^{charge}$ and $B_{\max}^{discharge}$ are the maximum charge and discharge rate of the HS (MWth), respectively.

2.1.12 Start-Up and Shut-Down Status Modeling for FC, CHP, and PO Units

The startup and shutdown modes of each CHP, FC, and ESS unit can be modeled by Eq. (33) and (34).

$$SU_h^i = V_h^i(1 - V_{h-1}^i), \qquad i \in \{FC, CHP, PO, HO\} \tag{2.33}$$

$$SD_h^i = (1 - V_h^i)V_{h-1}^i, \qquad i \in \{FC, CHP, PO, HO\} \tag{2.34}$$

where SU_h^i and SD_h^i denote startup and shutdown modes.

2.1.13 Time-of-Use-Based Demand Response Program (TOU-DRP)

To improve the cost-effectiveness of MEMG operation and reduce peak loads, time of use-based demand response program (TOU-DRP) is implemented. DR consumers shift electricity usage from high-price periods to low-price times, reducing generation costs and deferring infrastructure investments [23]. TOU-DRP is formulated by Eq. (35), and the amount of shifted load to h-th hour load level (i.e., ldr_h) is calculated by Eq. (36). It should be noted that the total amount of shifted load over a daily period is assumed to be equal to zero (See (37)). In addition, at each time period, demand response is limited by (38).

$$P_h^{DR} = P_h^D + ldr_h \tag{2.35}$$

$$ldr_h = DR_h P_h^D \tag{2.36}$$

$$\sum_{h=1}^{24} ldr_h = 0 \tag{2.37}$$

$$DR_h^{\min} \leq DR_h \leq DR_h^{\max} \tag{2.38}$$

where, ldr_{h} is the amount of shifted load to h-th hour load level, DR_h is the participation factor of the load in DRP in h-th load level, and P_h^D is the initial electric load demand in h-th load level (MWh).

2.2 Objective Functions

This study formulates two objectives as a multi-objective optimization problem, where the two conflicting goals are: (i) minimization of expected total operational cost (i.e., Expected Total Cost - TCost) and (ii) minimization of expected total pollutant emissions (i.e., Expected Total Emissions - ETEmission). It is worth mentioning that in case of considering the uncertainties in parameters, a set of scenarios are generated as mentioned in sub-section 2.1. Thus, these scenarios should be considered for the efficient solving of problem, and expected values are used to evaluate the effectiveness of uncertainty in each case study.

2.2.1 First Objective: Minimization of Total Cost

The first objective function, OF_1, represents the expected daily operational cost of the MEMG, including the following components: (i) revenue from selling electricity to the upstream grid, (ii) cost of purchasing electricity from the upstream grid, (iii) generation costs of CHP, FC, PO, and HO units, (iv) start-up and shut-down costs, and (v) battery degradation (as a ESS) costs. Eq. (39) represents the first objective function.

$$\begin{aligned} OF_1 = TCost_S = \sum_{h=1}^{24} \Bigg[& \lambda_h P_h^{G,buy} + \sum_{i=1}^{N_{CHP}} C(P_{i,h}^{CHP}, H_{i,h}^{CHP}) + C_{FC} \\ & + C(P_h^{PO}) + C(H_h^{HO}) + \sum_{j \in \{FC,CHP,PO,HO\}} (C_{j,SU} SU_h^j + C_{j,SD} SU_h^j) \\ & + C_k^{\deg} \sum_{k=1}^{N_k} \left(\frac{P_{k,h}^{dch}}{\eta_k^{dch}} + \eta_k^C P_{k,h}^C \right) - \lambda_h P_h^{G,sell} \Bigg] \end{aligned} \tag{2.39}$$

$$ETCost = \sum_{S=1}^{N_s} \pi_S \, TCost_S \tag{2.40}$$

where λ_h is the electricity price in h-th hour (\$/MWh), $P_h^{G,sell}$ and $P_h^{G,buy}$ are the amount of sold and purchased power to / from the upstream grid in h-th hour (MWh), respectively, $C\left(P_{i,h}^{CHP}, +H_{i,h}^{CHP}\right)$, C_{FC}, $C\left(P_h^{PO}\right)$, and $C\left(H_h^{HO}\right)$ are the CHP, FC, PO, and HO unit cost function (\$), respectively, $C_{j,SU}$ and $C_{j,SD}$ are startup and shutdown cost of generation facility (\$), respectively, SU_h^j and SD_h^j are binary variables of start-up or shut down modes for the units in h-th hour, $C_k^{\deg}$ is cost for battery degradation (\$/kWh), $P_{k,h}^{ch}$ and $P_{k,h}^{dch}$ are charged and discharged power of the battery (kW), respectively.

2.2.2 Second Objective: Minimization of Total Emissions

The second objective function, OF_2, aims to minimize the total daily emissions from generating units, expressed by Eq. (41). In order to consider uncertainties/scenarios, Eq. (42) is formulated. It should be mentioned that three main pollutants are considered as the emission components. And, according to ERGrid, the emission rate of grid values of NOx, CO2, and SO2 are 2.2952 kg/MWh, 921.25 kg/MWh and 3.5834 kg/MWh, respectively [28].

$$\begin{aligned} OF_2 = ETEmission_S &= \sum_{h=1}^{N_h} \left(E_h^{CHP} + E_h^{FC} + E_h^{PO} + E_h^{Grid}\right), \\ E_h^{CHP} &= \sum_{i=1}^{N_{CHP}} (NOx_{i,h} + SO2_{i,h} + CO2_{i,h}) = (k_1^{CHP} + k_2^{CHP} + k_3^{CHP}) P_{i,h}^{CHP}, \\ E_h^{FC} &= NOx_h^{FC} + SO2_h^{FC} + CO_h^{FC} = (k_1^{FC} + k_2^{FC} + k_3^{FC}) P_{i,h}^{FC}, \\ E_h^{PO} &= NOx_h^{PO} + SO2_h^{PO} + CO_h^{PO} = (k_1^{PO} + k_2^{PO} + k_3^{PO}) P_h^{PO}, \\ E_h^{Grid} &= NOx_h^{Grid} + SO2_h^{Grid} + CO2_h^{Grid} = (k_1^{Grid} + k_2^{Grid} + k_3^{Grid}) P_h^{Grid}. \end{aligned} \tag{2.41}$$

$$ETEmission = \sum_{S=1}^{N_s} \pi_S \, ETEmission_S \tag{2.42}$$

where $E_h^{CHP}, E_h^{FC}, E_h^{PO}$, and E_h^{Grid} are emission values of each unit (kg/day), respectively, NOx, SO_2, and CO_2 are pollutants considered as emission particles in this paper.

2.2.3 Fuzzy Decision-Making

In multi-objective optimization problems, after generating the Pareto optimal front (set), a planner needs to select a final solution from among the set of optimal solutions as the most balanced solution based on preferences or policy. To this end, the fuzzy min-max method assigns a fuzzy membership function to every solution within the Pareto front which is within the interval [0, 1], where $OF_{\text{k,p.u}} = 0$ indicates the worst possible selection while $OF_{\text{k,p.u}} = 1$ indicates the fully optimal solution. Eq. (43) is employed to urge fuzzy membership functions for the i-th objective function [33].

$$OF_{k,\text{p.u.}} = \begin{cases} 1, & OF_k \le OF_k^{\min}, \\ \dfrac{f_i^{\max} - f_i^k}{f_i^{\max} - f_i^{\min}}, & OF_k^{\min} < OF_k < OF_k^{\max}, \\ 0, & OF_k \ge OF_k^{\max}. \end{cases} \tag{2.43}$$

where ${f_i}^{\min}$ and ${f_i}^{\max}$ denote the minimum and maximum values for the i-th objective function among the non-dominated solutions, respectively.

In order to obtain the best final solution, the fuzzy decision making method is implemented. First, the minimum values of OF_1 and OF_2 are obtained, and then the solution with the maximum value of min (OF_1, OF_2) as the best final solution is selected.

2.3 Problem Constraints

So far, most of the problem constraints are expressed in modeling different components along with their formulations. However, remaining constrains are provided in the following.

2.3.1 Electrical Power Balance

With DRP, generated power should meet the load demand at each hour by (44).

$$P_h^{G,buy} - P_h^{G,sell} + \sum_{i=1}^{N_{CHP}} P_{i,h}^{CHP} + P_h^{FC} + P_h^{PO} + P_h^{dch} - P_h^{ch} - P_h^{DR} = 0, \qquad \forall h \tag{2.44}$$

where, P_h^{DR} is the electric load demand after applying DRP in h-th load level.

2.3.2 Thermal Power Balance

Balancing heat demand with the supply is another key requirement in MEMGs fulfilled by (45).

$$\sum_{i=1}^{N_{CHP}} H_{i,h}^{CHP} + H_h^{FC} + H_h^{HO} + H_h^{dch} - H_h^{ch} - H_h^{HS} = 0, \qquad \forall h \tag{2.45}$$

where, $H_{i,h}^{CHP}$ is heat generated by CHP unit in h-th hour, $H_h^{FC}$is recovered heat from FC in h-th hour, $H_h^{HO}$is generated heat by HO unit in h-th hour, H_h^{dch}discharged heat power from HS in h-th hour, and H_h^{ch} is charged (stored) heat into HS in h-th hour.

2.3.3 Grid Power Exchange

The electricity exchange between MEMG and upstream grid is limited by (46).

$$P_h^{Grid-\min} \leq P_h^{Grid} \leq P_h^{Grid-\max} \tag{2.46}$$

where $P_h^{Grid-min}$ and $P_h^{Grid-max}$ are minimum and maximum power exchange boundary between MEMG and upstream grid, respectively.

Operational constraints related to PO and HO units are previously defined by (16) and (17). Similarly, operational constraints of ESS are previously expressed by (23), (24), (25) and (26). Moreover, HS constraints are represented by (30), (31) and (32). Finally, TOU-DRP constraint has already given by (38).

3 Proposed Solution for the Optimization Problem

The multi-objective particle swarm optimization (MOPSO) algorithm has gained considerable popularity due to its remarkable efficiency in tackling optimization problems. The fundamental concept of MOPSO is derived from the collaborative behavior observed in nature, particularly the warm intelligence exhibited by animals [24]. MOPSO capitalizes on this natural phenomenon, employing particles that represent potential solutions to explore the search space and converge toward optimal or near-optimal outcomes by emulating these social dynamics. The algorithm has demonstrated notable success in addressing complex, nonlinear, multi-objective optimization problems [14]. In implementing MOPSO for optimization tasks, a population of particles is initialized, where each particle corresponds to a candidate solution. Within the search domain, each particle updates its position vector X_m according to its velocity vector V_m which reflects both its individual and collective learning experiences. The mathematical formulation for updating position and velocity vectors can be expressed by Eqs. (47). To enhance the performance of the energy system, an analytical approach is applied to refine the optimization process, ensuring both precision and computational efficiency. The velocity update is expressed by Eq. (48).

$$X_m^{k+1} = X_m^k + V_m^{k+1} \tag{3.1}$$

$$V_m^{k+1} = \omega V_m^k + c_1 r_1 (P_{best} - X_m^k) + c_2 r_2 (G_{best} - X_m^k) \tag{3.2}$$

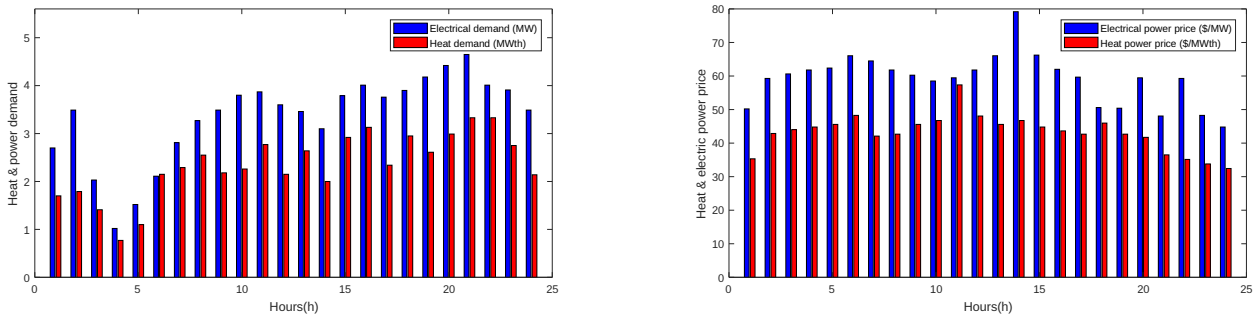
The objective is to minimize both operational cost and pollutant emissions simultaneously, subject to operational constraints and under uncertainty. The general form of a multi-objective optimization problem is defined by Eq. (49). The space within which the objective function is defined is called objective space. In multi-objective optimization, every two definitions can be described and have two different states with respect to each other as expressed in Eq. (50): (i) one solution can dominate the other one, (ii) no solution can dominate the other solution. In MOPSO algorithm, a repository is employed to save lots of solutions. Repository means an external memory on which the dominated solutions will be saved. This algorithm first starts to figure employing a series of random particles. All the population particles are compared with one another during a repeated procedure and position of the dominated particles is saved on the repository. To avoid redundancy and unnecessary use of space, interested readers may refer to Ref. [1], we used similarly the steps and flowchart of MOPSO algorithm implementation.

$$\begin{aligned} \min \;\; & F(\vec{X}) = [f_1(\vec{X}), f_2(\vec{X}), \ldots, f_N(\vec{X})]^T, \\ \text{subject to} \;\; & g_i(\vec{X}) < 0, \quad i = 1, 2, \ldots, N_{ueq}, \\ & g_i(\vec{X}) = 0, \quad i = 1, 2, \ldots, N_{eq}. \end{aligned} \tag{3.3}$$

$$\begin{aligned} &\forall j \in \{1, 2, \ldots, n\}, \quad f_j(\vec{X}_1) \leq f_j(\vec{X}_2), \\ &\exists k \in \{1, 2, \ldots, n\}, \quad f_k(\vec{X}_1) < f_k(\vec{X}_2). \end{aligned} \tag{3.4}$$

4 Case Studies and Simulation Results

The numerical values for emissions, FC parameters, ESS and HS characteristics, the startup and shutdown costs, and cost function coefficients of CHP along with the FOR data for the two types of CHP units are listed in [31]. The maximum demand shift by TOU-DRP is assumed to be 30%. The pollution coefficients of these power generation units are considered zero and the price of electricity generated by PV and WT units are 2.584 €ct/kwh and 1.073 €ct/kwh, respectively [33]. In addition, the maximum projected capacity for determining the capacity of PV and WT units are 1.5 MW and 1.2 MW, respectively. Figure 5 shows the base electrical (power) and thermal (heat) demand/price of MG.



(a) (b)

Figure 5: Electrical and thermal characteristics: (a) demand and (b) price.

To evaluate the proposed model, three case studies are analyzed:

- **Case A**: Islanded operation of the MEMG incorporating CHP, FC, PV, WT, PO, HO, HS and ESS,
- **Case B:** Grid-connected operation with the same configuration as Case A,
- **Case C**: Case B + Implementation of the TOU-DRP.

In Cases B and C, the MEMG is able to exchange (sell and/or purchase) power with the upstream network based on the dynamic market prices illustrated in Figure 5 (b). The optimization problem was solved in two phases. In the first phase, the MG operator used MOPSO algorithm to optimize MG operation based on the expected values derived from hourly average profiles of load, wind speed and solar irradiance. In this step, it is assumed that the electricity generated by PV and WT units must be purchased by the MG operator. In the second phase, uncertainty-based risk costs are minimized by the operator. A total of 1000 Monte Carlo-based scenarios were initially generated for the three uncertain parameters. Subsequently, a backward scenario reduction technique was applied, resulting in three representative scenarios per uncertainty. This process led to 27 (3*3*3) combined scenarios, for which expected total cost and expected emission cost were determined. Only the results of the Pareto solution front related to Scenario-S13 are presented as the scenario with the highest probability, and the results of other scenarios are presented in Table 6 once selected by the fuzzy decision-making method and the selected best compromise solution (See Figure 6) in order to calculate the expected total cost and expected total emissions.

4.1 Case A: Islanded Operation

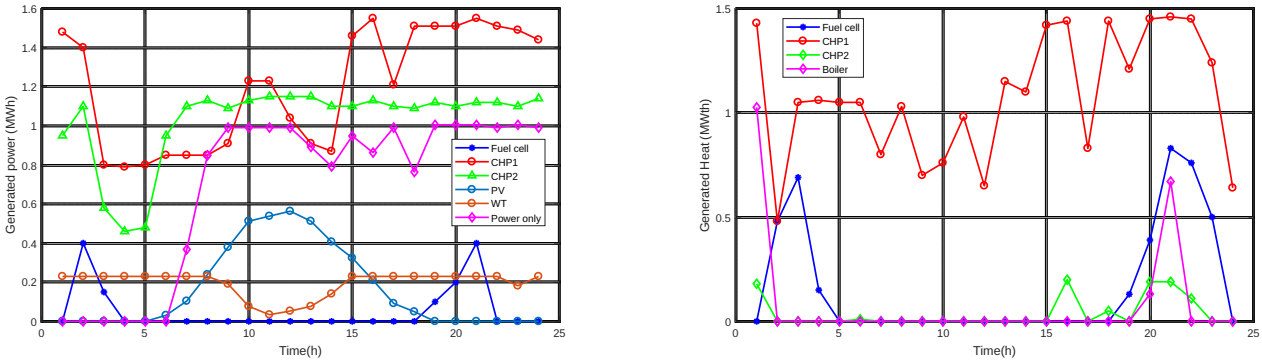
In the islanded operation mode, the MG operates autonomously without grid integration. Table 3 summarizes the Pareto optimal solutions for scheduling of MG neglecting TOU-DRP in Case A for Scenario-13. The minimum membership function of 0.6316 is obtained by Solution #13. Considering the min-max fuzzy satisfying method, Solution #13 is opted as the best compromise solution. That is, the cost of MG energy production is $4403.956, while, the amount of emission is obtained as 60984.88 kg/day. However, the minimum value of operation cost of MG

is obtained as \$4227.101, which is related to Solution #1 with the aim of minimizing the total cost of MG. Also, the minimum amount of emission provided is equal to 58962.319 kg/day, which is obtained by Solution #20 where the minimization of emission is aimed.

Figure 6 (a) illustrates the produced power by PV, WT, FC, CHP_1, and CHP_2 as well as PO units over 24 hours in Case A. As output of the optimization program, the production capacity of PV and WT units are 0.59 MW and 0.23 MW, respectively. The power production profiles of PV and WT units are shown in Figure 6 (a) over 24 hours in Case A. The supplied heat in Case A over the studied time horizon is illustrated in Figure 6 (b). Accordingly, the heat generation of CHP_1 is more than those of other production units. CHP_2 has less heat generation compared to CHP_1, since its heat cost is higher than that of CHP_1. The HO (i.e., boiler) and FC units have produced heat within their capacity limits. Looking at Figures 6 (a) and (b) and considering the time interval at which the FC has not participated in power and heat generation, the remained capacity of the FC is stored as hydrogen in the hydrogen tank at this time interval.

Table 3: Pareto-optimal solutions for short-term MEMG scheduling in Case A (Scenario S13).

Solution	OF_1 (\$/day)	OF_2 (kg/day)	OF_1 (p.u.)	OF_2 (p.u.)	$\min(OF_1, OF_2)$
1	4227.101	64452.02	1.0000	0.0000	0.0000
2	4235.8676	64163.666	0.9835	0.0525	0.0525
3	4244.1936	63874.724	0.9679	0.1052	0.1052
4	4252.5523	63585.54	0.9521	0.1578	0.1578
5	4261.7752	63296.797	0.9348	0.2104	0.2104
6	4276.3422	63007.939	0.9074	0.2631	0.2631
7	4291.9812	62718.826	0.8780	0.3157	0.3157
8	4307.2303	62430.055	0.8493	0.3683	0.3683
9	4322.8506	62141.996	0.8199	0.4208	0.4208
10	4338.6199	61851.76	0.7903	0.4737	0.4737
11	4355.4114	61562.876	0.7587	0.5263	0.5263
12	4384.4309	61273.689	0.7041	0.5790	0.5790
13	4403.956	60984.88	0.6674	0.6316	0.6316
14	4442.949	60695.647	0.5941	0.6843	0.5941
15	4472.1021	60407.017	0.5392	0.7368	0.5392
16	4506.2618	60117.995	0.4750	0.7895	0.4750
17	4569.3486	59829.367	0.3564	0.8421	0.3564
18	4679.5498	59540.568	0.1491	0.8947	0.1491
19	4719.3148	59251.478	0.0743	0.9473	0.0743
20	4758.8403	58962.319	0.0000	1.0000	0.0000



(a) (b)

Figure 6: Generated power and heat in Case A: (a) power generation and (b) heat generation.

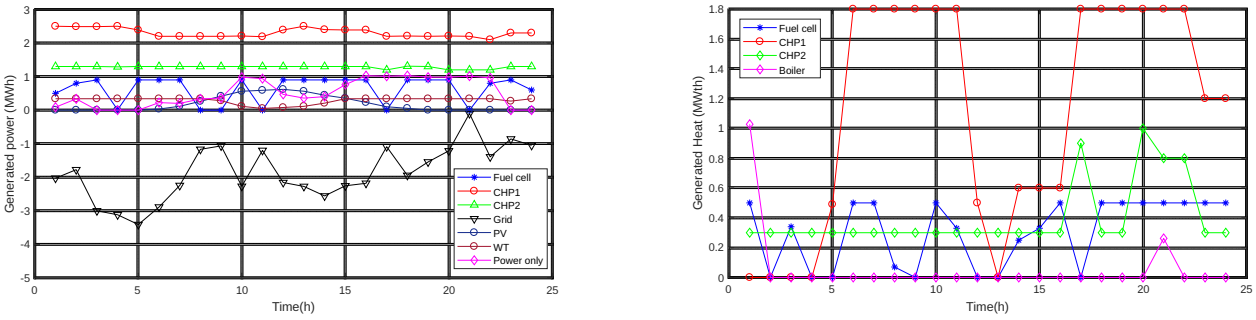
4.2 Case B: Grid-Connected Operation

Table 4 presents the Pareto optimal solutions in Case B for Scenario-S13. In this mode, the minimum membership function which is equal to 0.7416 is related to Solution #16. Taking into account the min-max fuzzy satisfying method, Solution #16 is selected as the best compromise solution. For this solution, the cost of MG energy production is \$3730.738, while, the emission amount is 55093.84 kg/day. In Solution #1, which is focused on the minimization of the total cost of MG, the minimum value of MG is obtained as S3702.019; whereas, Solution #20 aims to obtain the minimum emission amount which is equal to 53049.772 kg/day. Total operation cost of MG for in Case B compared to Case A decreased by about 15.3%, while the emission amount has decreased by about 9.7%. It means, when MG is connected to the network, the objectives are highly improved.

Table 4: Pareto-optimal solutions for short-term MEMG scheduling in Case B (Scenario S13).

Solution	OF_1 (\$/day)	OF_2 (kg/day)	OF_1 (p.u.)	OF_2 (p.u.)	min(OF_1, OF_2)
1	3702.019	62492.116	1.0000	0.0000	0.0000
2	3703.3005	62250.364	0.9885	0.0256	0.0256
3	3703.8511	61738.806	0.9835	0.0798	0.0798
4	3704.1196	61227.997	0.9811	0.1339	0.1339
5	3704.5965	60716.822	0.9768	0.1880	0.1880
6	3705.0845	60205.162	0.9724	0.2422	0.2422
7	3705.2673	59693.895	0.9708	0.2963	0.2963
8	3706.0203	59182.443	0.9640	0.3505	0.3505
9	3706.4356	58671.466	0.9603	0.4046	0.4046
10	3707.6484	58159.877	0.9494	0.4588	0.4588
11	3709.3555	57649.056	0.9340	0.5129	0.5129
12	3711.2299	57138.207	0.9171	0.5670	0.5670
13	3713.2289	56627.485	0.8991	0.6211	0.6211
14	3717.1511	56116.492	0.8639	0.6752	0.6752
15	3723.3446	55605.35	0.8081	0.7293	0.7293
16	3730.738	55093.84	0.7416	0.7835	0.7416
17	3740.8601	54583.002	0.6505	0.8376	0.6505
18	3755.9061	54071.861	0.5152	0.8918	0.5152
19	3776.0458	53560.572	0.3340	0.9459	0.3340
20	3813.1642	53049.772	0.0000	1.0000	0.0000

Figure 7 (a) and (b) depict the hourly power and heat production in Case B, respectively. Looking at Figure 7 (a), PV, WT, FC, CHP_1, and CHP_2 as well as PO unit have participated in power production in the scheduling over 24 hours. As the output of the optimization program, the production capacity of PV and WT units are 0.67 MW and 0.34 MW, respectively. The production profiles of PV and WT units are shown in this illustration over 24 hours. Considering the interconnection of MG and network, the MG has sold a part of power to the network. Moreover, CHP_1 and CHP_2 have contributed in power production continuously. With regard to Figure 7 (b), the heat production of CHP_1 unit is more than those of other production units, because generating power and heat by this unit is cheaper than the other units.



(a) (b)

Figure 7: Generated power and heat in Case B: (a) power generation and (b) heat generation.

4.3 Case C: Grid-Connected Operation Incorporating TOU-DRP

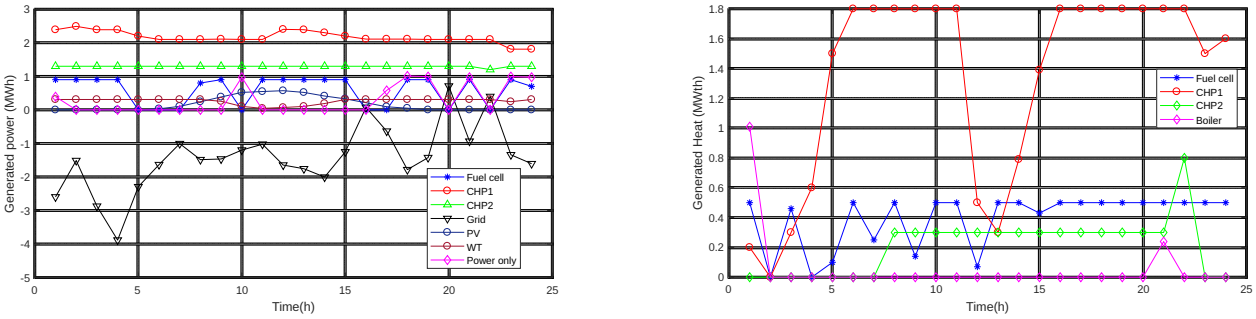
In Case C, the impact of incorporating the TOU-DRP in MG operation was assessed. Table 5 presents the Pareto optimal results for Scenario-S13. The minimum membership function is equal to 0.7687, which is related to Solution #16. According to the min-max fuzzy satisfying method, Solution #16 is the best compromise solution. The cost of MG energy production is \$3609.356 and the amount of emission is 54341.95 kg/day. However, in Solution #1, which is aimed to minimize operation cost, the final cost is \$3594.124. Also, when the emission minimization is aimed, the minimum value of operation emission is equal to 52712.029 kg/day that is related to Solution #20. Compared to the Case B, total operation cost in Case C has decreased by about 3.25% while the emission amount has decreased by about 1.37%. The results show the effectiveness of the TOU-DRP in grid-connected mode.

Figure 8 demonstrates the generated power and heat patterns in Case C incorporating TOU-DRP. As seen in Figure 8 (a), PV, WT, FC, CHP_1, and CHP_2 as well as PO unit have participated in power production in the scheduling

over 24 hours. As output of the optimization program, the production capacity of PV and WT units are 0.62 MW and 0.31 MW, respectively. The production curve of PV and WT units are shown over 24 hours. Considering the interconnection of MG and network, the MG has sold a part of generated power to the network and the MG has purchased a part of power from the network. Moreover, CHP_1 and CHP_2 have contributed in power production continuously. The heat generated in Case C for 24 hours is shown in Figure 8 (b). The participation of CHP_1 and FC in the heat generation of MG is obvious, in which CHP_1 has produced more heat than CHP_2 due to its low cost function. Additionally, CHP_2 and the boiler have less contribution to the heat generation in MG, since their cost functions are higher than those of other generation units. It should be noted that the generated hydrogen has been stored in the hydrogen tank.

Table 5: Pareto-optimal solutions for short-term MEMG scheduling in Case C (Scenario S13).

Solution	OF_1 (\$/day)	OF_2 (kg/day)	OF_1 (p.u.)	OF_2 (p.u.)	min(OF_1, OF_2)
1	3594.124	60189.17	1.0000	0.0000	0.0000
2	3594.1262	60047.954	1.0000	0.0189	0.0189
3	3594.59	59640.15	0.9929	0.0734	0.0734
4	3595.0403	59232.364	0.9861	0.1280	0.1280
5	3596.0522	58825.125	0.9707	0.1824	0.1824
6	3596.6727	58417.864	0.9613	0.2369	0.2369
7	3597.4428	58010.684	0.9496	0.2914	0.2914
8	3598.3417	57603.41	0.9360	0.3458	0.3458
9	3598.8486	57195.287	0.9283	0.4004	0.4004
10	3599.8584	56787.455	0.9129	0.4549	0.4549
11	3600.5629	56379.686	0.9022	0.5095	0.5095
12	3601.5667	55971.641	0.8870	0.5641	0.5641
13	3602.6033	55564.375	0.8713	0.6185	0.6185
14	3603.9396	55156.83	0.8510	0.6730	0.6730
15	3605.9495	54749.498	0.8205	0.7275	0.7275
16	3609.356	54341.95	0.7687	0.7820	0.7687
17	3615.4996	53934.708	0.6755	0.8365	0.6755
18	3621.9587	53527.247	0.5774	0.8910	0.5774
19	3634.8452	53120.039	0.3817	0.9454	0.3817
20	3659.9881	52712.029	0.0000	1.0000	0.0000



(a) (b)

Figure 8: Generated power and heat in Case C: (a) power generation and (b) heat generation.

The contribution of the of each component (i.e. FC, CHP1, CHP2, PV, WT and PO units) to electric energy generation for Scenario-S13 as a highest probability scenario is shown in Figure 9. The electric power demand for Case A and/or Case B is depicted in comparison with Case C in Figure 10. By applying TOU-DRP, load is shifted from high-price periods to inexpensive time periods. According to power prices shown in Figure 5, high-price periods are experienced between $h = 12$ and $h = 16$. Thus, TOU-DRP shifts load from these periods to inexpensive periods which are between $h = 22$ and $h = 24$. It should be denoted that the amount of these changes in TOU-DRP is limited by about 30%. Optimal Pareto solutions using MOPSO algorithm as well as selected trade-off solution based on fuzzy satisfying approach are shown in Figure 11.

5 Conclusions and Future Work

In this paper, the scheduling of a MEMG comprising of FC, two types of CHPs, a PO unit, PV, WT, HO unit, ESS and HS was investigated. A TOU-DRP was applied to manage power generation/demand more efficiently. To

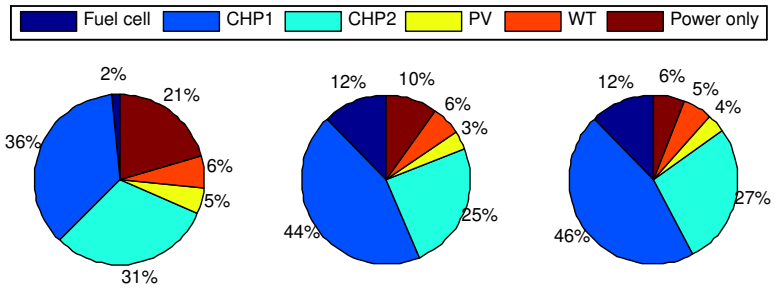


Figure 9: Percentage of electric power generation by the different MEMG components for Scenario S13: Case A, Case B, and Case C.

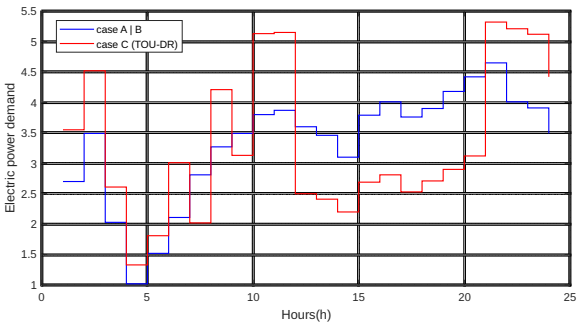


Figure 10: Electric power demand levels in Cases A/B compared with Case C.

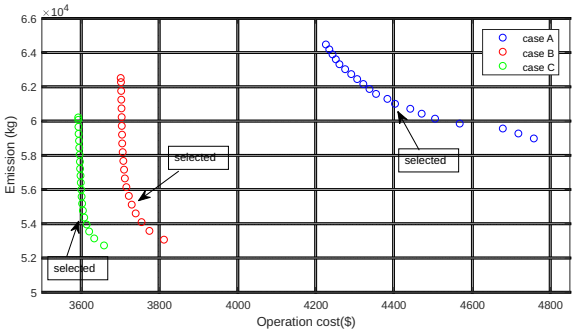


Figure 11: Pareto solution fronts obtained by MOPSO for Cases A, B, and C.

address uncertainties in load demand, wind speed and solar irradiation, a scenario-based stochastic modeling approach was employed, and expected value calculations were used to evaluate their impacts. The optimization problem, which considers minimization of both operational cost and emission cost was solved simultaneously using MOPSO algorithm. Pareto-optimal solutions were evaluated and ranked using the fuzzy min-max satisfaction method to identify the most suitable compromise solutions. In this study, three operational scenarios were analyzed to confirm the performance of the proposed approach, including islanded mode, grid-connected mode, and grid-connected mode with TOU-DRP. Over the 27 scenarios, the multi-objective optimization problem was implemented in MATLAB environment and the best solution was selected from the Pareto solution front by fuzzy decision making. In Case A, MEMG is considered in the islanded mode; and the expected operational cost and expected emission cost are achieved 4499.8 $/day and 61242.1 kg/day, respectively. In addition, in Case B, the expected operational cost and the expected emission cost are decreased to 3763.6 $/day and 57158.4 kg/day, respectively. Finally by implementing the TOU-DRP in Case C, the expected operational cost and expected emission cost of MEMG are reduced to 3632.7 $/day and 56014.4 kg/day, respectively. Compared to Case A, the minimization of operational cost and emission cost in Case B are improved by 9.7% and 15.3%. Nevertheless, results obtained in Case C revealed 3.25% and 1.37% improvements in operational costs and emissions, respectively, compared to Case B. It can be concluded that connecting the MEMG to the power grid reduces the operational and emission costs compared to the islanded mode. Also, using TOU-DRP helps to further improve these objective functions. As a future research work, the authors will consider uncertainties in other variables such as electricity price and device maintenance cost. In addition, correlation between random variables to produce quality samples will be studied.

Funding Statement

This article is derived from the author's doctoral dissertation at the university and has not received financial support from public, private, or non-profit organizations.

References

[1] G. R. Aghajani, H. A. Shayanfar, and H. Shayeghi, *Presenting a multi-objective generation scheduling model for pricing demand response rate in micro-grid energy management*, Energy Convers. Manag. **106** (2015), 308–321.

[2] E. Akhavan Maroofi, M. Samiei Moghaddam, A. Azarfar, R. Davarzani, and M. Vahedi, *A novel LSTPA methodology for managing energy in electrical/thermal microgrids through CHP, battery resources, thermal storage, and demand-side strategies*, Energy Inform. **8** (2025), no. 1, 1–29.

[3] L. Bagherzadeh, H. Shahinzadeh, H. Shayeghi, and G. B. Gharehpetian, *A short-term energy management of microgrids considering renewable energy resources, micro-compressed air energy storage and DRPs*, Int. J. Renew. Energy Res. **9** (2019), no. 4, 1712–1723.

[4] M. Bousla, M. Belfkir, A. Haddi, Y. E. Mourabit, and A. Sadki, *Comparative evaluation of Weibull parameter estimation methods for wind energy forecasting: A case study of the Tetouan wind farm with SCADA-based availability integration*, Results Eng. **27** (2025), 106835.

[5] H. Chen, S. Yang, H. Wu, J. Song, and S. Shui, *Advanced hierarchical energy optimization strategy for integrated electricity-heat-ammonia microgrid clusters in distribution network*, Int. J. Hydrogen Energy **97** (2025), 1481–1497.

[6] I. F. Davoudkhani, A. Dejamkhooy, and S. A. Nowdeh, *A novel cloud-based framework for optimal design of stand-alone hybrid renewable energy system considering uncertainty and battery aging*, Appl. Energy **344** (2023), 121257.

[7] S. Dorahaki, S. M. Muyeen, and N. Amjady, *A Stackelberg game theory model for integrated community energy storage systems*, IEEE Access **12** (2024), 152908–152920.

[8] A. Esparza, M. Blondin, and J. P. F. Trovão, *A review of optimization strategies for energy management in microgrids*, Energies **18** (2025), no. 13, 3245.

[9] P. Farhadi and S. M. M. Tafreshi, *Optimum management of manual sectionalizers in electric power distribution networks integrating distributed generations using binary exchange market algorithm*, Int. J. Energy Sect. Manag. (2020).

[10] P. Farhadi, M.-T. Seyed-Masoud, and A. Shahirinia, *A comprehensive review on stochastic modeling of electric vehicle charging load demand regarding various uncertainties*, Smart Sci. **12** (2024), no. 4, 679–714.

[11] M. Gheydi, P. Farhadi, and R. Ghafari, *The effect of demand response on operation of smart home energy system with renewable energy resources*, *2016 Int. Symp. Fundam. Electr. Eng. (ISFEE)* (2016).

[12] I. L. R. Gomes, R. Melicio, and V. M. F. Mendes, *A novel microgrid support management system based on stochastic mixed-integer linear programming*, Energy **223** (2021), 120030.

[13] M. Hadi, E. Elbouchikhi, Z. Zhou, and A. Saim, *Optimal energy management in multi energy microgrid with combined heat and power system and demand side response integration*, Renew. Energy **256** (2026), 124076.

[14] A. Hadj Slama, L. Saidi, M. Saidi, and M. Benbouzid, *Metaheuristic optimization of hybrid renewable energy systems under asymmetric cost-reliability objectives: NSGA-II and MOPSO approaches*, Symmetry **17** (2025), no. 9, 1412.

[15] R. Hasani, M. Mohammadi, and A. Samanfar, *Integrated multiobjective energy management for a smart microgrid incorporating electric vehicle charging stations and demand response programs under uncertainty*, Int. J. Energy Res. **2025** (2025), no. 1, 9531493.

[16] Z. M. Hassan, M. M. El-Saadawi, A. Y. Hatata, P. Sanjeevikumar, and B. E. Sedhom, *Leveraging modified golden jackal optimization for enhanced demand-side management in microgrids with different tariffs*, Energy Rep. **13** (2025), 3672–3685.

[17] L. He, Z. Lu, L. Pan, H. Zhao, X. Li, and J. Zhang, *Optimal economic and emission dispatch of a microgrid with a combined heat and power system*, Energies **12** (2019), no. 4, 604.

[18] P. Horrillo-Quintero, P. García-Triviño, C. E. Ugalde-Loo, E. Hosseini, C. A. García-Vázquez, M. Tostado, F. Jurado, and L. M. Fernández-Ramírez, *Efficient energy dispatch in multi-energy microgrids with a hybrid control approach for energy management system*, Energy **317** (2025), 134599.

[19] M. M. Ibrahim, H. M. Hasanien, H. E. Z. Farag, and W. A. Omran, *Energy management of multi-area islanded hybrid microgrids: A stochastic approach*, IEEE Access **11** (2023), 101409–101424.

[20] K. Jalilpoor, S. Nikkhah, M. S. Sepasian, and M. G. Aliabadi, *Application of precautionary and corrective energy management strategies in improving networked microgrids resilience: A two-stage linear programming*, Electr. Power Syst. Res. **204** (2022), 107704.

[21] D. Kanakadhurga and N. Prabaharan, *Demand side management in microgrid: A critical review of key issues and recent trends*, Renew. Sustain. Energy Rev. **156** (2022), 111915.

[22] P. Li, M. Jiang, Y. Zhang, and Y. Zhang, *Cooperative optimization of bus service and charging schedules for a fast-charging battery electric bus network*, IEEE Trans. Intell. Transp. Syst. **24** (2023), no. 5, 5362–5375.

[23] M. Majidi, S. Nojavan, and K. Zare, *Optimal stochastic short-term thermal and electrical operation of fuel cell/photovoltaic/battery/grid hybrid energy system in the presence of demand response program*, Energy Convers. Manag. **144** (2017), 132–142.

[24] H. Manafi, N. Ghadimi, M. Ojaroudi, and P. Farhadi, *Optimal placement of distributed generations in radial distribution systems using various PSO and DE algorithms*, Elektron. Elektrotech. **19** (2013), no. 10, 53–57.

[25] F. Moazzen and M. J. Hossain, *A two-layer strategy for sustainable energy management of microgrid clusters with embedded energy storage system and demand-side flexibility provision*, Appl. Energy **377** (2025), 124659.

[26] M. Nazari-Heris, S. Abapour, and B. Mohammadi-Ivatloo, *Optimal economic dispatch of FC-CHP based heat and power micro-grids*, Appl. Therm. Eng. **114** (2017), 756–769.

[27] T. Niknam, R. Azizipanah-Abarghooee, and M. R. Narimani, *An efficient scenario-based stochastic programming framework for multi-objective optimal micro-grid operation*, Appl. Energy **99** (2012), 455–470.

[28] A. Ramadan, M. Ebeed, S. Kamel, A. Y. Abdelaziz, and H. Haes Alhelou, *Scenario-based stochastic framework for optimal planning of distribution systems including renewable-based DG units*, Sustainability **13** (2021), no. 6, 3566.

[29] S. Satish kumar, V. Pramila, S. Rudhra, S. Vinod, and D. Lakshmi, *Enhancing demand response and energy*

management in multi-microgrid systems with renewable energy sources, Renew. Energy **253** (2025), 123490.

[30] H. Shuai, J. Fang, X. Ai, J. Wen, and H. He, *Optimal real-time operation strategy for microgrid: An ADP-based stochastic nonlinear optimization approach*, IEEE Trans. Sustain. Energy **10** (2019), no. 2, 931–942.

[31] M. Taghizadeh, S. Bahramara, F. Adabi, and S. Nojavan, *RETRACTED: Optimal operation of storage-based hybrid energy system considering market price uncertainty and peak demand management*, J. Energy Storage **30** (2020), 101519.

[32] V. Thang and N. Trung, *Probabilistic optimization of planning and operation of networked microgrids with renewable energy resources considering demand response programs*, Energy Syst. **16** (2025), no. 1, 91–110.

[33] Q. Wei, D. Liu, Y. Liu, and R. Song, *Optimal constrained self-learning battery sequential management in microgrid via adaptive dynamic programming*, IEEE/CAA J. Autom. Sin. **4** (2017), no. 2, 168–176.

[34] J. Ye, Q. Shuai, and Q. Hua, *Dynamic programming-based low-carbon and economic scheduling of integrated energy system*, Energy **322** (2025), 135568.

[35] P. Zare, A. Dejamkhooy, and I. F. Davoudkhani, *Efficient expansion planning of modern multi-energy distribution networks with electric vehicle charging stations: A stochastic MILP model*, Sustain. Energy Grids Netw. **38** (2024), 101225.

[36] X. Zheng, F. Bai, and T. Jin, *Assessing customer-side demand response identification for optimal scheduling considering satisfaction level for microgrids*, Int. J. Electr. Power Energy Syst. **164** (2025), 110368.